AD-A126 616 IMAGING RECEIVER FOR TARGET REFERENCING OF ADAPTIVE OPTICAL SYSTEMS: PERF..(U) DEFENCE RESEARCH ESTABLISHMENT VALCARTIER (QUEBEC) 1/1

UNCLASSIFIED L R BISSONNETTE ET AL. MAR 83 F/G 17/8 NL

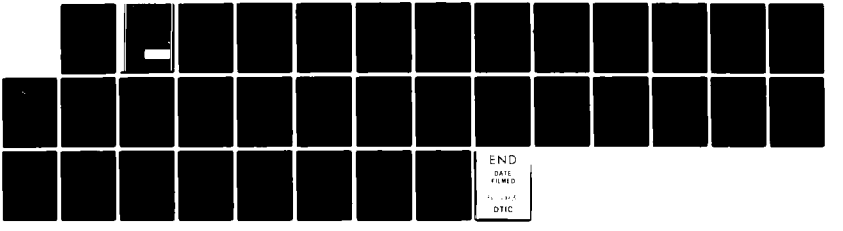

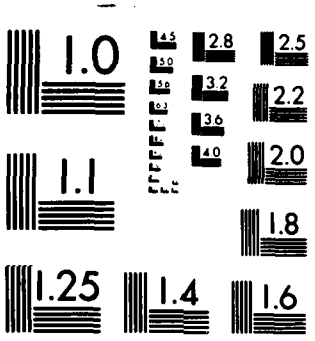

DREV REPORT 4292/83
FILE: 3633B-007
MARCH 1983

CRDV RAPPORT 4292/83
DOSSIER: 3633B-007
MARS 1983

IMAGING RECEIVER FOR TARGET REFERENCING OF ADAPTIVE OPTICAL SYSTEMS: PERFORMANCE AND COMPARISON WITH PREDICTIONS

L. R. Bissonnette

N. Blais

Centre de Recherches pour la Défense
Defence Research Establishment
Valcartier, Québec

DREV R-4292/83
FILE: 3633B-007

UNCLASSIFIED

CRDV R-4292/83
DOSSIER: 3633B-007

IMAGING RECEIVER FOR TARGET REFERENCING OF ADAPTIVE OPTICAL SYSTEMS: PERFORMANCE AND COMPARISON WITH PREDICTIONS

by

L. R. Bissonnette and N. Blais*

* Co-op student, Université de Sherbrooke

CENTRE DE RECHERCHES POUR LA DEFENSE
DEFENCE RESEARCH ESTABLISHMENT
VALCARTIER
Tel: (418) 844-4271

Québec, Canada

March/mars 1983

ABSTRACT

The imaging method for target referencing of adaptive optics systems in the presence of extended targets in turbulence is compared with the conventional method which assumes an unresolved glint target. The tests were performed with a tilt-compensation system. There is a degradation due to the imaging process, but the technique still gives satisfactory results well into the scintillation saturation region. The gain measurements agree well with the predictions based on the propagation model developed at Defence Research Establishment Valcartier (DREV).

RÉSUMÉ

On compare la méthode d'imagerie pour l'asservissement des systèmes d'optique adaptable en présence de cibles non ponctuelles dans l'atmosphère turbulente à la méthode conventionnelle qui suppose une cible petite non résolue. Les essais ont été effectués avec un système de stabilisation du pointage. On observe un affaiblissement du gain causé par le processus d'imagerie à travers la turbulence, mais la méthode donne quand même des résultats satisfaisants jusque dans la région de saturation de la scintillation. Les mesures de gain concordent avec les solutions calculées à partir du modèle de propagation mis au point au Centre de recherches pour la défense, Valcartier (CRDV).

TABLE OF CONTENTS

1.0 INTRODUCTION

The propagation of laser beams in the earth's atmosphere is greatly affected by the random fluctuations of the refractive index produced by the air turbulence. The principal effects relevant to this study are beam wander and beam spreading. Beam wander describes the random steering of the beam by the large turbulent eddies of the atmosphere. Beam spreading is an average phenomenon whereby the smaller eddies act as scatterers that laterally diffuse the beam. Both effects contribute to an average power density loss at the target.

In many applications, these turbulence effects can be corrected by the recently developed technique of adaptive optics (Refs. 1 and 2 provide an extensive review). In principle, an adaptive laser transmitter senses the phase distortions induced by the atmosphere, and applies in real time the corresponding correction to an active optical component. Several devices have been proposed and built to apply this general concept. The one such system that offers the best advantages for beam control, and appears to be technologically more advanced, is called the multidither outgoing-wave (MDOW) system (Refs. 3 and 4). The principal characteristics of the MDOW system are that the phase errors are measured by the transmitted beam, and that the separate controllable active elements are identified by dithering at different frequencies.

The phase-error sensing method of the MDOW device is indirect and based on the return by the target of a fraction of the transmitted radiation. The servo loop acts to maximize the retroreflected signal. Obviously, the system converges and compensates for the turbulence-induced power density losses only if the detected signal is proportional to the irradiance of the transmitted beam on the target.

This condition requires that the target area scattering back most of the radiation be smaller than the incident beam, i.e. not resolved by the transmitter optics. It is the scenario usually assumed for applications.

In a preceding report (Ref. 5), we have shown that the method can be successfully extended to resolved targets by imaging the target laser pattern on a pinhole aperture, thus creating an artificial glint. The significant finding was that the proposed imaging receiver works in turbulent media beyond the limited range predicted by the classic theory on resolution and isoplanatism. The analysis of the artificial glint approach is pursued further in this report. It compares the tilt-compensation gain produced under the same turbulence conditions by a two-degree-of-freedom MDOW system referenced by a conventional physical glint, and by the proposed artificial glint. The results are analyzed in the light of recent published models on the fading effect of anisoplanatism. Also, the tilt-correction data are compared with calculations based on a propagation model developed at Defence Research Establishment Valcartier (DREV), Refs. 6-7.

Chapter 2.0 reviews the theoretical background and chapter 3.0 describes the experiment. Chapter 4.0 compares the system performance to predictions derived from recent literature models. Finally, the solutions from the DREV model are discussed in chapter 5.0.

This work was performed at DREV between January and June 1982 under the PCN 33B07, Atmospheric Propagation of a Laser Beam.

2.0 THEORETICAL BACKGROUND

In the conventional physical-glint approach, the MDOW feedback loop is closed by simply collecting the radiation retroreflected by an unresolved feature on the target. The proposed artificial-glint technique for resolved objects consists in imaging the target laser pattern on a pinhole aperture. The pinhole thus defines a point on the image of the laser spot, and the detected signal is proportional to the irradiance at the conjugate object point on the target. In principle, this satisfies the basic requirement for target referencing. The concept is obvious except for the influence of the intervening turbulent medium which degrades the imaging process.

The instantaneous resolving power of an imaging system in turbulence is almost diffraction limited, but the position of the object point fluctuates continuously and randomly. On the average, the object point covers a domain of area L given by

$$L = (\lambda z)^2/\pi\rho_o^2, \qquad [1]$$

where λ is the wavelength of the transmitted beam, z is the propagation distance, and ρ_o is the phase coherence length first introduced by Fried (Ref. 8). For propagation over a path with homogeneous turbulence strength, which constitutes a convenient simplification for the present analysis, ρ_o is given by

$$\rho_o = (1.09\ k^2\ z\ C_n^2/n_o^2)^{-3/5}, \qquad [2]$$

where k is the optical wave number of the laser beam, C_n is the turbulence refractive index structure parameter, and n_o is the refractive index of the unperturbed propagation medium. The area L

defines the long-term resolution in turbulence.

According to the phenomenon just described, the signal detected through the pinhole of the imaging optics remains proportional to the target irradiance, but at a point that keeps wandering. In other words, the artificial glint defined by the imaging system changes position randomly. Therefore, for an MDOW feedback loop to remain effective under such conditions, it is required that the extent of the turbulence-induced excursions of the object point be smaller than the area S of coherence of the transmitted beam. Otherwise, there would be less and less causal relationship between the feedback signal and the quantity it is meant to control. From conventional theory, the area S is given by

$$S = \pi\rho_o^2. \qquad [3]$$

Hence, the resulting necessary condition for the validity of the proposed artificial glint in the case of extended targets in turbulence is

$$L < S, \qquad [4]$$

which yields

$$(\lambda z/\pi\rho_o^2)^2 = (1.94\ k^{7/6}\ z^{11/6}\ C_n^2/n_o^2)^{12/5} < 1. \qquad [5]$$

In terms of the amplitude fading distance, i.e.

$$z_A = n_o^{12/11}/C_n^{12/11}\ k^{7/11}, \qquad [6]$$

the criterion becomes

$$(z/z_A)^{22/5} < 0.2, \qquad [7]$$

i.e. $z/z_A < 0.7$, which is about half way into the weak perturbation region. For example, if we assume a 3-km propagation range, the limiting turbulence strength C_n^2 at 3.8 and 10.6 μm is 1.2 and 4×10^{-14} $m^{-2/3}$, respectively. These values can easily be exceeded by daytime ground-level turbulence.

An equivalent condition was derived by Shapiro (Ref. 9) in relation to the adaptive processing of images of extended targets through turbulence. In his case, S is defined as the area of the isoplanatic patch which is also given by eq. 3. The difference in concept stems from the method of probing the atmosphere. In his application, the turbulence state is measured by the signal emitted from the object whereas in the outgoing-wave approach studied here, this is done by the beam transmitted to the target. For linear media, the two methods are equivalent and should indeed be subject to approximately the same restrictions.

3.0 EXPERIMENT

The experiment was carried out in laboratory-generated turbulence. The refractive-index turbulence is produced by creating an unstable vertical temperature gradient in a tank filled with water (Refs. 10-11). This is done simply by heating the water at the bottom of the tank and cooling it at the top. The turbulence develops naturally and fits quite well the Kolmogoroff inertial subrange. The C_n value can be easily controlled in the range of 10^{-5} to 10^{-4} $m^{-1/3}$. The tank is 1.6 m long, 0.6 m deep and 0.4 m wide. The propagation path can be increased by folding the beam lengthwise.

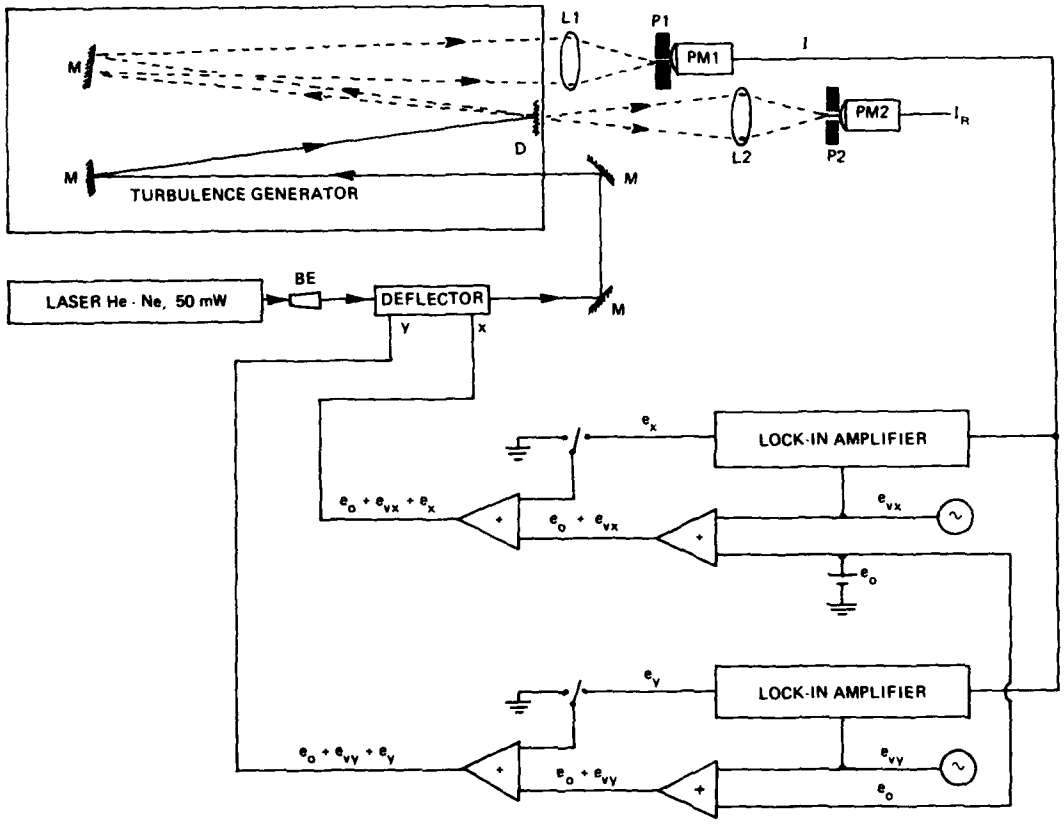

FIGURE 1 - Experimental setup for testing the proposed imaging technique on a tilt-compensation MDOW adaptive optics system.

BE: beam expanding and focusing optics; M: plane mirror;
D: uniformly diffusing target;
L1: f = 300 mm, f/4; P1: pinhole aperture, 100 μm;
L2: f = 200 mm, f/2.5; P2: pinhole aperture, 50 μm;
PM1 and PM2: photomultipliers.

The tests were performed with a two-degree-of-freedom MDOW system designed for tilt correction. The experimental arrangement is sketched in Fig. 1. The active optical component consists of two Bragg cells that deflect the transmitted beam in two orthogonal x and y directions. The Bragg cells are driven by voltage-controlled high-frequency acoustic oscillators (VCO). A constant deflection is imposed by the adjustable bias voltage e_o to separate the diffraction orders at the entrance window to the turbulence generator. Only the (1,1) beam is allowed to propagate in the turbulence, it is focused on the target positioned at a distance z measured in the turbulence. The target is a thin uniformly diffusing plastic sheet, it is truly extended and does not produce a glint.

The target laser pattern is probed by the imaging system L1P1 looking through the turbulence along a noncollinear but equal distance path. The lens L1 has a focal length f = 300 mm, an aperture f/4, and a magnification (i/o) ≈ 0.3 where i stands for image size and o, for object size. The pinhole P1 has a diameter of 100 μm. This gives a geometrical resolution in the object plane of 330 μm, which is about half the measured aberrated but nonturbulent beam spot, and smaller than the turbulence-degraded average profile by a factor ranging from 3 to 18 for the conditions investigated. For reference measurements, a second imaging system L2P2 probes the same laser spot through the nonturbulent air.

The x-channel is dithered at a frequency of 200 Hz and a peak-to-peak amplitude of about 0.1 mrad. The y-channel is similarly dithered but at a frequency of 300 Hz. The signal from the imaging system L1P1 is synchronously processed by two lock-in amplifiers tuned respectively at 200 and 300 Hz. The output voltages of the lock-in

amplifiers are added to the VCO inputs of the corresponding deflectors to close the loop. The parameters adjusted to optimize the loop operation were the phase reference, sensitivity, and time constant of the lock-in amplifiers. For several results reported here, both channels were dithered at the same frequency (250 Hz) but in phase quadrature. In such cases, the processing was made by a single lock-in amplifier that provides in-phase and quadrature outputs. No further modifications were required.

The tests with the physical glint were simulated by substituting a point detector (10-μm aperture) in place of the diffusing target of Fig. 1. The system operation was otherwise unchanged.

4.0 EXPERIMENTAL RESULTS

Illustrative results with the artificial-glint referencing are shown in Fig. 2 where sample recordings of the irradiance signal detected by the reference imaging system are reproduced. For these data, both imaging systems L1P1 and L2P2 were aligned to probe the same point on the target. For Fig. 2a, this point was chosen at the center of the beam profile. As can be seen, the closing of the loop causes an increase in the average irradiance. For the recording of Fig. 2b, the beam was originally displaced so that the imaging system probed a point located on the side of the beam spot in open-loop conditions, more precisely at a radial position equal to 3 times the radius at e^{-1} of the open-loop average irradiance profile. At the instant the servo loop is activated, we observe that the beam is automatically recentered and remains so, even if we vary e_o or turn a steering mirror. Therefore, the MDOW tilt-compensation system operates effectively with the proposed imaging receiver, it corrects for the turbulence-induced beam wander, and can track the artificial glint. These recordings were

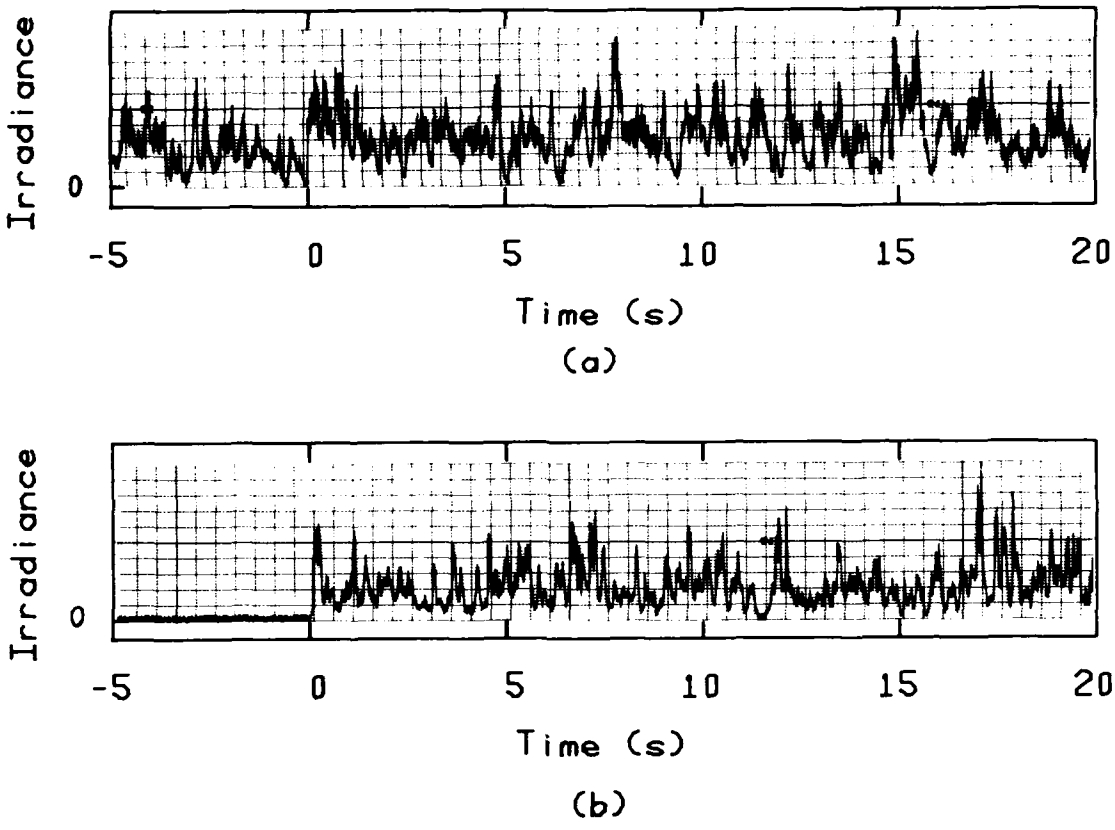

FIGURE 2 - Sample time recordings of the irradiance signal detected by the reference imaging system. Time zero corresponds to the closing of the servo-loop. (a) - the artificial glint is defined on the axis of the open-loop beam; (b) - the artificial glint is defined on the side of the open-loop beam at a radial position equal to 3 times the 1/e-radius of the open-loop target irradiance profile.
$C_n/n_o = 9.0 \times 10^{-5}\ m^{-1/3}$; $z = 2.95$ m; $z/z_A = 3.9$.

made for $z/z_A = 3.9$, while the theoretical limit set by eq. 7 is 0.7. Hence, the validity criterion based on the classic measures of resolution and coherence (or isoplanatism) is not borne out by the data of Fig. 2.

Following these results and others reported in Ref. 5, a more systematic survey of the system performance was carried out. The wander-corrected on-axis irradiance gain was determined for various turbulence and beam conditions. The same experiment was repeated twice: first, under the control of the proposed artificial glint and second, under the control of the conventional physical glint. In each case and for each set of parameters, the on-axis average irradiance was successively measured in open- and closed-loop conditions. The gain was calculated from the ratio of the latter to the former. The signals were recorded digitally, and the averages computed from 3-min long samples. In the closed-loop mode, the feedback inputs to the deflectors were also recorded, which allowed the calculation of the average and the variance of the corrected beam displacements.

The gain results are plotted in Fig. 3 versus z/z_A, where z is the propagation distance and z_A, the amplitude fading range given by eq. 6. The parameter z/z_A is certainly not the sole parameter affecting the tilt compensation gain, but it appears satisfactory for the present purpose of regrouping the data.

The data of Fig. 3 show that the gain is smaller with the artificial glint than with the physical glint. This is to be expected since the process of imaging through turbulence certainly causes some degradation. It is also important to note that both sets of data follow the same pattern over the whole domain investigated. The gain

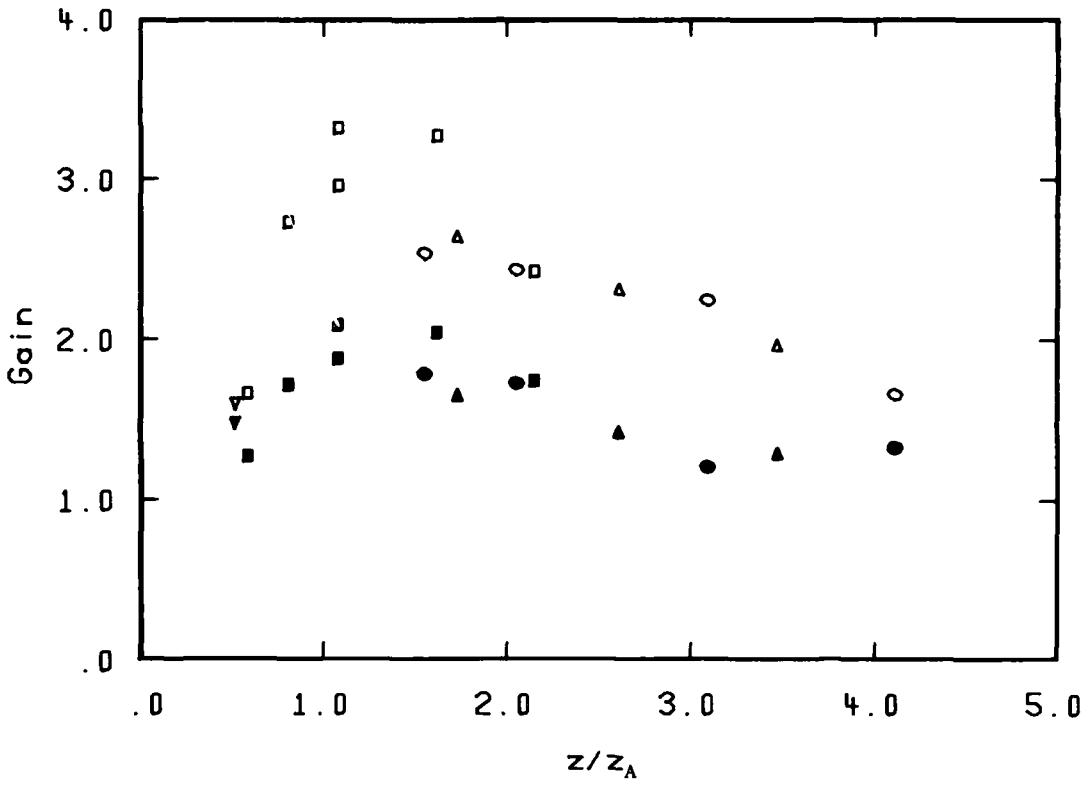

FIGURE 3 - Measured on-axis tilt-compensation gain. The open symbols are for the conventional physical-glint referencing; the solid symbols, for the proposed artificial-glint referencing.

▼ and ▽: z = 1.00 m, w_o = 1.35 mm;

■ and □: z = 1.57 m, w_o = 1.90 mm;

▲ and △: z = 2.53 m, w_o = 2.31 mm; and

● and ○: z = 3.00 m, w_o = 2.44 mm.

initially increases, reaches a maximum at $z/z_A \approx 1.5$, and then slowly decreases with increasing turbulence effect. In other words, the artificial-glint method does not behave differently from the conventional physical-glint technique. The peak performance is reached at a propagation range more than twice as far as the theoretical limit of $z/z_A \approx 0.7$ and the system continues to operate satisfactorily, compared with the physical-glint performance, much beyond this limit.

A full-range comparison with theory, as opposed to the simple limit criterion of eq. 7, concerns the ratio of the artificial-glint to the physical-glint tilt-compensation gain. The data are plotted in Fig. 4. This ratio measures the fading effect of the artificial-glint method. The gain degradation is due to the loss of coherence in the distorted target laser profile since it is probed, by the process of imaging through the turbulence, at a position that instantaneously differs from the aimpoint. On a return-wave system, the corresponding and equivalent effect would be that of anisoplanatism. Fried (Ref. 12) has recently developed a theoretical model for this effect, and found that it depends on two main parameters: the normalized aperture diameter d/r_o of the transmitted beam and the normalized angular separation θ/θ_o between the aimpoint and the reference glint, where

$$r_o = 3.18\ \rho_o, \text{ and} \qquad [8]$$

$$\theta_o = \rho_o/z. \qquad [9]$$

Fried's model can be applied to the present situation, at least qualitatively. For Gaussian beams, his diffraction-limited antenna gain formula implies that d is equal to the beam diameter at e^{-4} in irradiance. However, our acousto-optic deflector, with its four cylindrical lenses, has aberrations that make the undistorted focal-

plane beam spot greater than the diffraction limit by a factor of 3.3. To account for this, we simply divide by 3.3 the value of d at the transmitter. The effect is to reduce the amount of fading predicted by the theory. For the separation angle θ, we take the half-angle subtended by the point-spread area L. It is recalled that L delimits the average domain of the random excursions of the object point which defines the artificial glint. Thus, θ is the average separation angle between the instantaneous position of the artificial glint and the aimpoint of the transmitted beam. This definition of θ agrees with that of Fried. From eqs. 1 and 9, it thus follows that

$$\theta = \frac{1}{z}\sqrt{\frac{L}{\pi}} = \frac{\lambda}{\pi\rho_o}, \qquad [10]$$

$$\frac{\theta}{\theta_o} = \frac{\lambda z}{\pi\rho_o^2}. \qquad [11]$$

The parameter pairs d/r_o and θ/θ_o were determined for each set of experimental conditions investigated. The fading values were then computed by interpolation from the tabulated fading function in Table 1 of Ref. 12. The results are plotted as a continuous curve in Fig. 4. Actually, all the points do not fall on a single curve since they depend on two parameters. However, the differences between the plotted average curve and the calculated values are less than 5% for the conditions of the present experiment. Considering the measurement errors, these differences are negligible, and the single curve is well justified.

The comparison of Fried's curve with the experimental data illustrates and supplements the simple criterion of eq. 7. We observe that the measurements approximately follow the predictions up to

$z/z_A \simeq 1$ where they level off as opposed to the theoretical curve which begins to drop rapidly. The breaking point agrees well with that derived from eq. 7. For $z/z_A > 1$, the measured fading remains nearly constant between 60 and 70%. By contrast, the predicted fading is down to 4.5% at $z/z_A = 2$ and keeps decreasing.

Fried's model of anisoplanatism gain fading was developed for full adaptive optics compensation. It is expected that tilt correction, which is of interest here, is less degraded by anisoplanatism. This was analyzed by Valley (Ref. 13). The governing parameters are basically the same as in Fried's model. They were determined as described earlier and the gain degradation was calculated from the eqs. 8, and 12 to 16 of Ref. 13. The results are plotted in Fig. 4, and again the single curve fits all the calculated values within 5%. As illustrated, the tilt compensacion is indeed less degraded by anisoplanatism. However, the trend is similar. After a slower decrease for $z/z_A < 2$, the drop rate becomes comparable to that of the full compensation curve. Clearly, neither of the theoretical curves supports the measured leveling off of the gain fading. This leveling off implies that the proposed artificial-glint concept remains a practical target-referencing method at propagation ranges extending far into the scintillation saturation region.

The reason for the disagreement is difficult to establish with certainty. The theoretical models of Fried and Valley, and the criterion of eq. 7 all depend on the measure of the coherence or the isoplanatism domain. In all cases, this is obtained by assuming a single-scale amplitude covariance function. The scale is given by ρ_o multiplied by a constant factor of order unity. It was verified in Ref. 5 that ρ_o is indeed the appropriate scale at small separation distance for the present application of a focused-beam outgoing-wave

tilt-compensation system. However, the same measurements also show that, in the saturation region, the initial drop of the covariance function is followed by a long residual correlation tail whose scale is much greater than ρ_o, and increases relative to ρ_o with increasing turbulence strength. Neglecting this second scale surely contributes to an underestimation of the coherence or the isoplanatism domain. However, it remains to be determined whether this is sufficient to fully account for the stable and satisfactory performance of the artificial-glint technique in the saturation region, as demonstrated in Figs. 2-4. Unfortunately, no adequate model of the residual correlation phenomenon yet exists. This constitutes one of the remaining difficulties of the turbulence theory which is beyond the scope of the present report. Nevertheless, the effect of this second scale on the calculation of the isoplanatic domain appears significant, and may well explain the discrepancies of Fig. 4. It is certainly worth investigating in future studies.

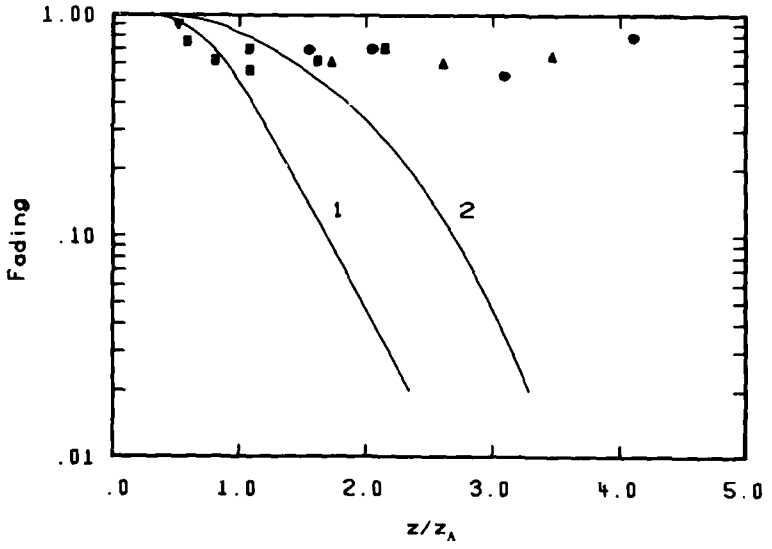

FIGURE 4 - Measured gain fading compared with the models of Fried (curve No. 1) and Valley (curve No. 2). Data symbols as defined in Fig. 3.

5.0 MODEL PREDICTIONS

The theoretical model developed at DREV for laser beam propagation in turbulence (Ref. 14) includes the effect of adaptive optics (Refs. 6 and 7). The calculation results for perfect tilt compensation are compared with the physical-glint data in Fig. 5. The predictions are represented by a single curve. This is not exact since the solution depends on three similarity parameters besides the normalized propagation distance z/z_A. However, the experimental conditions are such that all the calculated points corresponding to the data of Fig. 5 are well fitted by the drawn average curve, the differences are less than 5% of the local values.

At small z/z_A, the data follow the theoretical curve quite well. But, for $z/z_A > 1$, the experiment shows a saturation of the tilt-compensation gain whereas the predicted gain continues to increase, although less rapidly. There is even a supersaturation phenomenon since the measured gain slowly decreases beyond its maximum level at $z/z_A \simeq 1.5$. The calculations were performed for exact phase retrieval and ideal phase-conjugate implementation at the tilt-correction order.

Simultaneously to the irradiance measurements, the feedback signals to the active deflectors were recorded. These allowed the calculation of the corrected beam wander. According to the classic theory, the beam wander variance is given by (Ref. 15)

$$\sigma^2_{b.w.} = 2.91\ b^{-1/3}\ \frac{C_n^2}{n_o^2}\ z^3, \qquad [12]$$

where b is the beam diameter. For Gaussian beams, it is customary to take $b = 2\sqrt{2}\ w_o$, where w_o is the beam radius at e^{-1}. Hence from

eq. 12, it follows that

$$\frac{\sigma_{b.w.}}{w_o} = 1.43 \frac{C_n z^{3/2}}{n_o w_o^{7/6}}. \qquad [13]$$

Equation 13 is compared with the physical-glint data in Fig. 6. Again, we observe that the data fit quite well the theoretical curve at small propagation distance or turbulence strength before saturating at a level approximately equal to 0.25. This constitutes further evidence, based on classic theoretical results, that the gain attainable with a tilt-compensation system saturates compared with the ideal beam-wander correction. Thus, the discrepancy of Fig. 5 is not an artifact of our computation model. The degradation is attributed to the scintillation effect which is modeled in the following paragraphs.

The computation algorithm of the effect of adaptive optics is based on the following expression (Ref. 6):

$$\underset{\sim}{v}_o(\underset{\sim}{r}_i) = \frac{1}{\sigma_i} \iint_{\sigma_i} d^2\rho\, W_i(\underset{\sim}{\rho}) \{\underset{\sim}{v}_b(\underset{\sim}{r}_i+\underset{\sim}{\rho}) - \Gamma_i(\underset{\sim}{\rho})\underset{\sim}{v}_t(\underset{\sim}{r}_i+\underset{\sim}{\rho})\}, \qquad [14]$$

which relates the phase front angle $\underset{\sim}{v}_o$ implemented by the i^{th} element of the active optical component to the instantaneous phase front angle $\underset{\sim}{v}_t$, at the transmitter, of the spherical wave retroreflected by a target glint or emitted by a reference beacon. $W_i(\underset{\sim}{\rho})$ is the influence function of the i^{th} element, $\Gamma_i(\underset{\sim}{\rho})$ is a correlation function and $\underset{\sim}{v}_b$ is an independent random vector function representing the system noise. Equation 14 is a general linear relationship between $\underset{\sim}{v}_o$, the implemented wavefront, and $\underset{\sim}{v}_t$, the exact reference wavefront. As formulated, it models a return-wave system. However, for linear distortions such as produced by refractive index turbulence, the

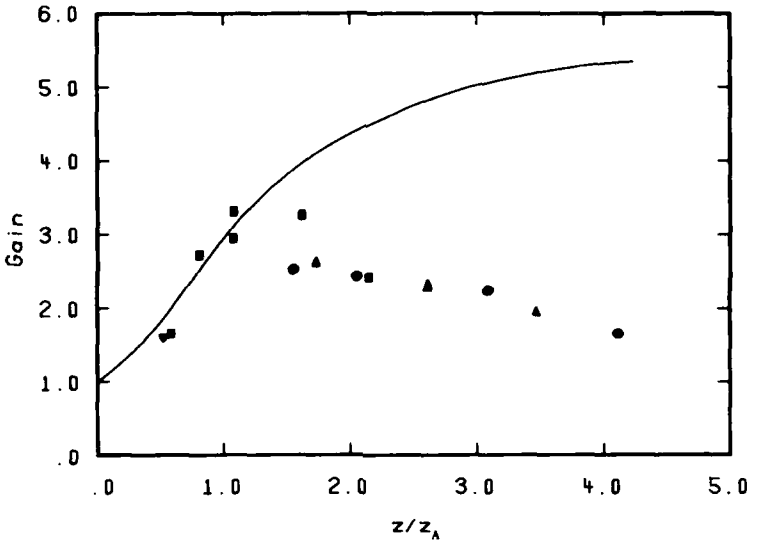

FIGURE 5 - Calculated ideal tilt-compensation irradiance gain (———) compared with the data in the case of the conventional physical-glint referencing. Data symbols as defined in Fig. 3.

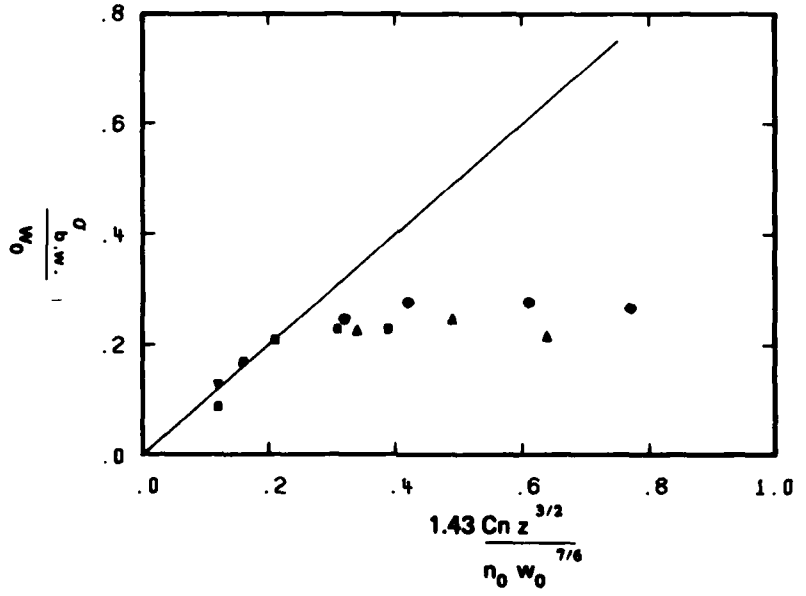

FIGURE 6 - Theoretical beam wander (———) compared with the measured tilt corrections in the case of the conventional physical-glint referencing. Data symbols as defined in Fig. 3.

return-wave and the outgoing-wave systems are equivalent (Ref.2, p. 255). Hence, eq. 14 is also applicable to the present situation.

For the calculations illustrated in Fig. 5 we have assumed an ideal system , i.e. $\Gamma = 1$ and $\underset{\sim}{v}_b = 0$. In the following calculations, we will suppose the noise equal to the dither modulation, i.e.

$$\sigma_b = \langle \underset{\sim}{v}_b \cdot \underset{\sim}{v}_b \rangle^{\frac{1}{2}} = 50 \ \mu\text{rad}, \qquad [15]$$

which represents a lower limit. The noise reduces the gain performance by an amount that varies only slightly with z/z_A and therefore cannot explain the saturation phenomenon of Figs. 5 and 6.

The measured gain saturation occurs quite suddenly. At $z/z_A \simeq 1$, the data of both Figs. 5 and 6 deviate abruptly from the calculated curves. Based on this behavior and on the examination of the beam pattern, we propose that the scintillation-induced fading of the tilt-correction gain comes mainly from the beam breakup phenomenon which begins to appear at $z/z_A \simeq 1$. The separation of the beam into individual and almost independent random patches is likely to confuse the MDOW feedback loop. Indeed, we expect the system to instantaneously lock on to one patch and ignore the others. Since the wandering of the beam centroid depends on the motion of all the patches, the correction achieved by tracking a single patch is certainly less than for true-centroid wander compensation. The position, size, and strength of the patches change with time so that the system probably keeps hopping between them, adding to the gain degradation. The confusion surely grows with the number N of these patches. In the framework of our model, this confusion is measured by the correlation coefficient Γ, and it therefore appears reasonable to set Γ inversely proportional to N, i.e.

$$\Gamma \propto 1/N. \qquad [16]$$

Experiments by Raidt and Höhn (Ref. 16) have shown that the size of the individual patches is equal to the diffraction-limited beam size. However, to estimate their number, we must allow for their separate wandering and stretching under the conditions of the experiment, i.e. with the tilt-compensation system on. In the same way as the patch size constitutes the turbulence-free resolution of the transmitter, we assume that the average area occupied by a single patch in the absence of scintillation fading constitutes the fundamental or unaberrated resolution of the adaptive system under study. Hence, for the present application, we relate this area to the average beam area calculated for perfect tilt correction. Therefore, the number N of patches that cannot be eliminated at the tilt-compensation order, owing to scintillation fading, is approximated by

$$N \simeq w^2(\Gamma,\sigma_b)/w^2(1,0), \qquad [17]$$

where w stands for the focal plane average beam radius calculated for tilt correction under parameters Γ and σ_b shown in parentheses. From eqs. 16 and 17, it follows that

$$\Gamma \propto \frac{w^2(1,0)}{w^2(\Gamma,\sigma_b)}. \qquad [18]$$

The proportionality factor missing in eq. 18 cannot be constant. On the one hand, if it were constant and equal to unity, the ideal condition $\Gamma = 1$ would be a solution of eq. 18 in the limit $\sigma_b \to 0$ regardless of the turbulence level, which cannot be. On the other hand, if we let the proportionality factor be different from unity, eq. 18 will not satisfy the limiting solution $\Gamma = 1$ for vanishing turbulence strength and σ_b. Therefore, the proportionality factor

must be a function of the scintillation strength. The simplest model is a linear relationship which gives

$$\Gamma = [1 - \varepsilon\ \beta(1,0)]\ \frac{w^2(1,0)}{w^2(\Gamma,\sigma_b)}, \qquad [19]$$

where β is the focal plane scintillation contrast, i.e. the ratio of the irradiance standard deviation to the average irradiance, and ε is a constant coefficient to be determined empirically. Equation 19 satisfies the solution $\Gamma = 1$ in the limits $\sigma_b \to 0$ and $\beta \to 0$.

Equation 19 is an implicit equation for parameter Γ, it must be solved numerically by iterations. The method is straightforward and generally converges after three or four iterations. However, we have experienced a few cases where the solution is sensitive to errors in the calculated beam radii. This occurs when the curve $y = [1-\varepsilon\beta]\ w^2(1,0)/w^2(\Gamma,\sigma_b)$ versus Γ crosses the line $y = \Gamma$ almost tangently.

The computation results are compared with the physical-glint data in Fig. 7. The coefficient ε was set equal to 0.1 and was not further adjusted. Two curves are drawn corresponding to two sets of experimental conditions. The agreement with the data is very good. The measured saturation and supersaturation of the tilt-compensation gain are well reproduced by the theoretical curves.

For the artificial-glint referencing, it was shown in the preceding section that there is additional fading associated with the process of imaging through the turbulence. This effect is mostly independent of the scintillation fading. Hence, the values of Γ calculated for the physical-glint referencing need only be multiplied by a derating factor. It was verified in Fig. 4 that the existing models cannot provide a suitable estimate of this factor. We must

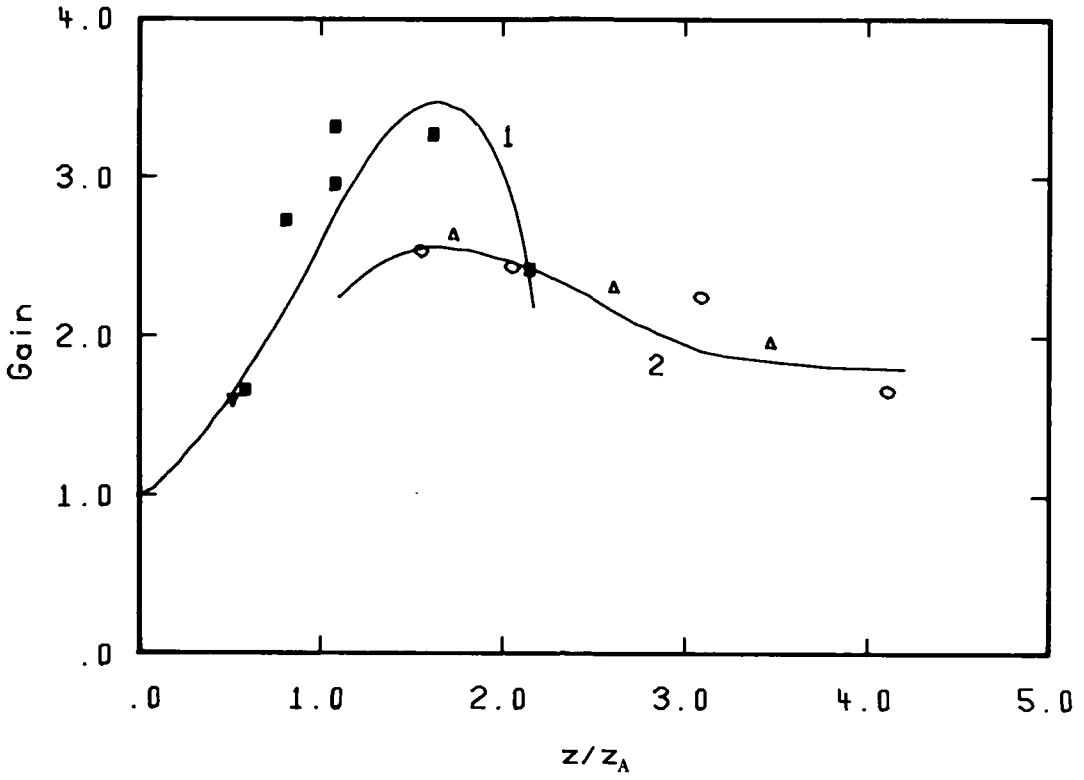

FIGURE 7 - Calculated tilt-compensation gain (———) accounting for the irradiance-scintillation fading compared with the data in the case of the conventional physical-glint referencing.
Curve No. 1: $z = 1.57$ m, $w_o = 1.90$ mm;
Curve No. 2: $z = 3.00$ m, $w_o = 2.44$ mm.
Data symbols as defined in Fig. 3.

resort to experimental data, and the parameter that comes to mind is the correlation coefficient, measured in Ref. 5, between the target irradiance and the signal derived from the imaging receiver that defines the artificial glint. This coefficient quantifies the level of confidence in the suitability of the artificial glint to constitute a proper MDOW referencing channel. This concurs with the definition or the interpretation of Γ. Therefore, the Γ's of Fig. 7 were simply multiplied by the correlation coefficients obtained from Ref. 5, i.e. 0.65 for the 1.57-m propagation range, and 0.60 for the 3.00-m range. The calculation results are plotted in Fig. 8. Again, the agreement with the data is excellent.

The proposed model for the scintillation-induced gain fading, namely eqs. 14 and 19, is well corroborated by the present experiment. However, it constitutes only an initial attempt at modeling a rather complex phenomenon. It requires more extensive verification, in particular with multi-degree-of-freedom MDOW adaptive optics systems. We hope that such data could become available to pursue this analysis.

6.0 CONCLUSION

In a preceding report (Ref. 5), we have shown that an imaging receiver can provide a suitable target reference for the control of MDOW adaptive optics systems in the case of extended targets in turbulence. The technique was further tested here with a two-degree-of-freedom system. In particular, the performance of the proposed artificial-glint method was determined by comparing its tilt compensation gain to that measured under the control of a physical glint. As expected, there is some degradation but the gain remains nearly constant at 60-70% for all turbulence conditions investigated, i.e. up to $z/z_A = 4.1$. This result contrasts with the recent models of Fried (Ref. 12) and Valley (Ref. 13) which predict a rapid fading of

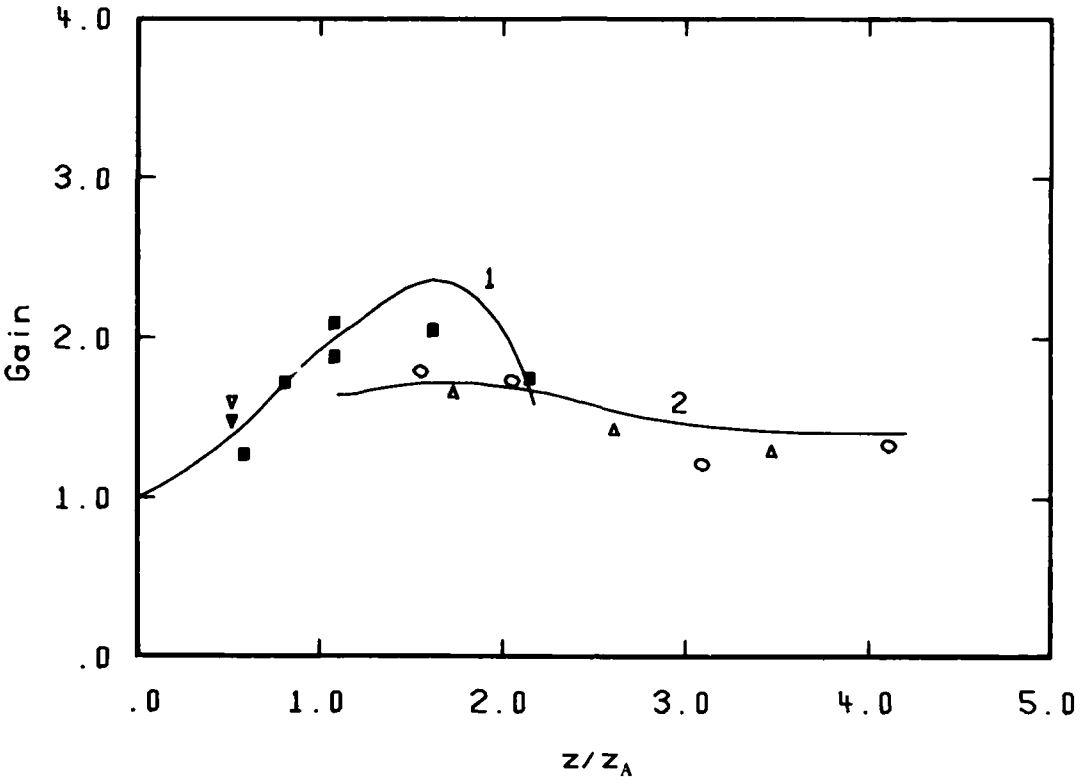

FIGURE 8 - Calculated tilt-compensation gain (———) accounting for the irradiance-scintillation fading compared with the data in the case of the artificial-glint referencing. Curves and data symbols as defined in Fig. 7.

the gain, below practical levels, for $z/z_A > 1$ and $z/z_A > 2$, respectively. The reason for the apparent theoretical overestimation of the fading effect has not yet been fully established but it is probably related to the problem of the proper coherence scale or scales. In particular, the models assume a single-scale amplitude covariance function and neglect the residual correlation tail observed in the saturation regime. This approximation underestimates the coherence domain, but further theoretical studies are needed to determine if it is sufficient to explain the observed discrepancies. Additional experimentation in the atmosphere and with higher order adaptive systems is also required.

The tilt-compensation gain measured with the physical-glint referencing was compared with the calculations based on the propagation model developed at DREV. The results show a saturation of the gain beginning with the saturation of the irradiance scintillation. This fading was attributed to the effect of scintillation. A model was worked out which explains the degradation by the difficulty for the MDOW tilt-tracking algorithm to distinguish between the overall beam centroid and that of the individual patches formed when the beam starts to breakup. In the computational framework, this effect reduces the correlation between the implemented phase front and the conjugate of the reference phase front by a quantity inversely proportional to the number of separate patches in the beam. The resulting solutions agree very well with the data. However, the proposed model of scintillation-induced gain fading still requires extensive testing, especially with higher order compensation systems.

7.0 ACKNOWLEDGEMENTS

The authors are pleased to acknowledge the able technical assistance of A. Perreault and R. Rochette. Many thanks are also extended to M. Gravel for helpful discussions.

8.0 REFERENCES

1. Hardy, J.W., "Active Optics: A New Technology for the Control of Light", Proc. of the IEEE, Vol. 66, No. 6, pp. 651-697, 1978.

2. Pearson, J.E., Freeman, R.N. and Reynolds, H.C. Jr., "Adaptive Optical Techniques for Wave-Front Correction", in Applied Optics and Optical Engineering, Vol. 7, Robert R. Shannon and James C. Wyant eds., Academic Press, New York, 1979.

3. Pearson, J.E., Bridges, W.B., Hansen, S., Nussmeier, T.A. and Pedinoff, M.E., "Coherent Optical Adaptive Techniques: Design and Performance of an 18-element Visible Multidither COAT System", Appl. Opt., Vol. 15, No. 3, pp. 611-621, 1976.

4. O'Meara, T.R., "The Multidither Principle in Adaptive Optics", J. Opt. Soc. Am., Vol. 67, No. 3, pp. 306-315, 1977.

5. Bissonnette, L.R., "Outgoing-Wave Optical Adaptive Systems in the Presence of Extended Diffuse Targets in Turbulence", DREV R-4262/82, May 1982, UNCLASSIFIED

6. Bissonnette, L.R., "Propagation Model of Adaptively Corrected Laser Beams in Turbulence", DREV R-4200/81, October 1981, UNCLASSIFIED

7. Bissonnette, L.R., "Propagation of Adaptively Corrected Laser Beams through a Turbulent Atmosphere", Journal de physique, Colloque C9, supplément au no. 11, Tome 41, p. C9-415, novembre 1980.

8. Fried, D.L. "Statistics of a Geometric Representation of Wavefront Distortion", J. Opt. Soc. Am., Vol. 55, No. 11, pp. 1427-1435, 1965.

9. Shapiro, J.H., "Diffraction-Limited Atmospheric Imaging of Extended Objects"., J. Opt. Soc. Am., Vol. 66, No. 5, pp. 469-477, May 1976.

10. Bissonnette, L.R., "Laboratory Simulation of Atmospheric Turbulence for Optical Propagation Studies", DREV R-4075/77, August 1977, UNCLASSIFIED

11. Bissonnette, L.R., "Atmospheric Scintillation of Optical an Infrared Waves: A Laboratory Simulation"., Appl. Opt., Vol. 16, No. 8, pp. 2242-2251, 1977.

12. Fried, D.L., "Anisoplanatism in Adaptive Optics", J. Opt. Soc. Am., Vol. 72, No. 1, pp. 52-61, 1982.

13. Valley, George C., "Isoplanatic Degradation of Tilt Correction and Short-Term Imaging Systems", Appl. Opt., Vol. 19, No. 4, pp. 574-577, 1980.

14. Bissonnette, L.R., "Focused Laser Beams in Turbulent Media", DREV R-4178/80, December 1980, UNCLASSIFIED

15. Tatarskii, V.I., "Wave Propagation in a Turbulent Medium", Chapt. 13, Dover Publications, New York, 1967.

16. Raidt, H. and Höhn, D.H., "Instantaneous Intensity Distribution in a Focused Laser Beam at 0.63 μm and 10.6 μm Propagating through the Atmosphere", Appl. Opt., Vol. 14, No. 11, pp. 2747-2749, 1975.

CRDV R-4292/83 (NON CLASSIFIE)

Bureau - Recherche et Développement, MDN, Canada
CRDV, C.P. 8800, Courcelette, Qué. G0A 1R0

"Méthode d'imagerie pour l'asservissement des optiques adaptables: performance et comparaison avec les calculs" par L.R. Bissonnette et N. Blais

On compare la méthode d'imagerie pour l'asservissement des systèmes d'optique adaptable en présence de cibles non ponctuelles dans l'atmosphère turbulente à la méthode conventionnelle qui suppose une cible petite non résolue. Les essais ont été effectués avec un système de stabilisation du pointage. On observe un affaiblissement du gain causé par le processus d'imagerie à travers la turbulence, mais la méthode donne quand même des résultats satisfaisants jusque dans la région de saturation de la scintillation. Les mesures de gain concordent avec les solutions calculées à partir du modèle de propagation mis au point au Centre de recherches pour la défense, Valcartier (CRDV).

CRDV R-4292/83 (NON CLASSIFIE)

Bureau - Recherche et Développement, MDN, Canada
CRDV, C.P. 8800, Courcelette, Qué. G0A 1R0

"Méthode d'imagerie pour l'asservissement des optiques adaptables: performance et comparaison avec les calculs" par L.R. Bissonnette et N. Blais

On compare la méthode d'imagerie pour l'asservissement des systèmes d'optique adaptable en présence de cibles non ponctuelles dans l'atmosphère turbulente à la méthode conventionnelle qui suppose une cible petite non résolue. Les essais ont été effectués avec un système de stabilisation du pointage. On observe un affaiblissement du gain causé par le processus d'imagerie à travers la turbulence, mais la méthode donne quand même des résultats satisfaisants jusque dans la région de saturation de la scintillation. Les mesures de gain concordent avec les solutions calculées à partir du modèle de propagation mis au point au Centre de recherches pour la défense, Valcartier (CRDV).

CRDV R-4292/83 (NON CLASSIFIE)

Bureau - Recherche et Développement, MDN, Canada
CRDV, C.P. 8800, Courcelette, Qué. G0A 1R0

"Méthode d'imagerie pour l'as*ervissement des optiques adaptables: performance et comparaison avec les calculs" par L.R. Bissonnette et N. Blais

On compare la méthode d'imagerie pour l'asservissement des systèmes d'optique adaptable en présence de cibles non ponctuelles dans l'atmosphère turbulente à la méthode conventionnelle qui suppose une cible petite non résolue. Les essais ont été effectués avec un système de stabilisation du pointage. On observe un affaiblissement du gain causé par le processus d'imagerie à travers la turbulence, mais la méthode donne quand même des résultats satisfaisants jusque dans la région de saturation de la scintillation. Les mesures de gain concordent avec les solutions calculées à partir du modèle de propagation mis au point au Centre de recherches pour la défense, Valcartier (CRDV).

CRDV R-4292/83 (NON CLASSIFIE)

Bureau - Recherche et Développement, MDN, Canada
CRDV, C.P. 8800, Courcelette, Qué. G0A 1R0

"Méthode d'imagerie pour l'asservissement des optiques adaptables: performance et comparaison avec les calculs" par L.R. Bissonnette et N. Blais

On compare la méthode d'imagerie pour l'asservissement des systèmes d'optique adaptable en présence de cibles non ponctuelles dans l'atmosphère turbulente à la méthode conventionnelle qui suppose une cible petite non résolue. Les essais ont été effectués avec un système de stabilisation du pointage. On observe un affaiblissement du gain causé par le processus d'imagerie à travers la turbulence, mais la méthode donne quand même des résultats satisfaisants jusque dans la région de saturation de la scintillation. Les mesures de gain concordent avec les solutions calculées à partir du modèle de propagation mis au point au Centre de recherches pour la défense, Valcartier (CRDV).

DREV R-4292/83 (UNCLASSIFIED)

Research and development Branch, DND, Canada
DREV, P.O. Box 8800, Courcelette, Que. GOA 1RO

"Imaging Receiver for Target Referencing of Adaptive Optical Systems: Performance and Comparison with Predictions" by L.R. Bissonnette and N. Blais

The imaging method for target referencing of adaptive optics systems in the presence of extended targets in turbulence is compared with the conventional method which assumes an unresolved glint target. The tests were performed with a tilt-compensation system. There is a degradation due to the imaging process, but the technique still gives satisfactory results well into the scintillation saturation region. The gain measurements agree well with the predictions based on the propagation model developed at Defence Research Establishment Valcartier (DREV).

DREV R-4292/83 (UNCLASSIFIED)

Research and development Branch, DND, Canada
DREV, P.O. Box 8800, Courcelette, Que. GOA 1RO

"Imaging Receiver for Target Referencing of Adaptive Optical Systems: Performance and Comparison with Predictions" by L.R. Bissonnette and N. Blais

The imaging method for target referencing of adaptive optics systems in the presence of extended targets in turbulence is compared with the conventional method which assumes an unresolved glint target. The tests were performed with a tilt-compensation system. There is a degradation due to the imaging process, but the technique still gives satisfactory results well into the scintillation saturation region. The gain measurements agree well with the predictions based on the propagation model developed at Defence Research Establishment Valcartier (DREV).

DREV R-4292/83 (UNCLASSIFIED)

Research and development Branch, DND, Canada
DREV, P.O. Box 8800, Courcelette, Que. GOA 1RO

"Imaging Receiver for Target Referencing of Adaptive Optical Systems: Performance and Comparison with Predictions" by L.R. Bissonnette and N. Blais

The imaging method for target referencing of adaptive optics systems in the presence of extended targets in turbulence is compared with the conventional method which assumes an unresolved glint target. The tests were performed with a tilt-compensation system. There is a degradation due to the imaging process, but the technique still gives satisfactory results well into the scintillation saturation region. The gain measurements agree well with the predictions based on the propagation model developed at Defence Research Establishment Valcartier (DREV).

DREV R-4292/83 (UNCLASSIFIED)

Research and development Branch, DND, Canada
DREV, P.O. Box 8800, Courcelette, Que. GOA 1RO

"Imaging Receiver for Target Referencing of Adaptive Optical Systems: Performance and Comparison with Predictions" by L.R. Bissonnette and N. Blais

The imaging method for target referencing of adaptive optics systems in the presence of extended targets in turbulence is compared with the conventional method which assumes an unresolved glint target. The tests were performed with a tilt-compensation system. There is a degradation due to the imaging process, but the technique still gives satisfactory results well into the scintillation saturation region. The gain measurements agree well with the predictions based on the propagation model developed at Defence Research Establishment Valcartier (DREV).

END

DATE
FILMED

5 — 83

DTIC